New Evidence against Hydroxyl Radicals as Reactive Intermediates in the Thermal and Photochemically Enhanced Fenton Reactions

Stefan H. Bossmann,* Esther Oliveros, Sabine Göb, Silvia Siegwart, Elizabeth P. Dahlen, Leon Payawan, Jr., Matthias Straub, Michael Wörner, and André M. Braun

Lehrstuhl für Umweltmesstechnik, Engler-Bunte-Institut, Universität Karlsruhe, D-76128 Karlsruhe, Germany

Received: November 7, 1997; In Final Form: February 10, 1998

During the oxidative degradation of 2,4-dimethylaniline (2,4-xylidine) by means of the H_2O_2/UV method, a series of hydroxylated aromatic amines are formed, this result confirming the role of the hydroxyl radical as an initiator of the oxidative chain reaction. Thermal or photochemically enhanced Fenton reactions in the presence of 2,4-dimethylaniline (2,4-xylidine) yield primarily 2,4-dimethylphenol as an intermediate product, the genesis of which may only be explained by an electron transfer mechanism. Experimental evidence for such a mechanism is presented, and values for the quantum yields of the photochemically enhanced reduction of iron(III) to iron(II) in aqueous solutions of 2,4-xylidine are given.

Introduction

Photochemical degradation processes (also referred to as advanced oxidation processes, AOP) have been proposed in recent years for the treatment of ground, surface, and wastewaters containing biocidal or nonbiodegradable organic compounds.[1] AOP are mainly based on oxidative degradation reactions, most often initiated by hydroxyl radicals which may be generated by various methods (e.g. UV photolysis of hydrogen peroxide, TiO_2 photocatalysis, vacuum ultraviolet (VUV) photolysis of water).[1,2] Among AOP, the Fenton reaction[3] and especially the photochemically enhanced Fenton reaction are considered most promising for the remediation of highly contaminated waters. A wide range of applications have been reported,[4,5] including the successful treatment of industrial wastewaters on a large pilot scale (500 L) by the photochemically enhanced Fenton reaction.[6]

Although the Fenton reagent (a mixture of hydrogen peroxide and iron(II) salt) has been known for more than a century[3a,b] and proven long since a powerful oxidant, the mechanism of the Fenton reaction is still under intense and controversial discussion. According to the classic interpretation of Haber and Weiss,[7] the reaction of iron(II) with hydrogen peroxide (H_2O_2) in aqueous solution leads to the formation of a hydroxyl radical ($HO^\bullet$) (reaction 1.1). In 1951, Barb et al.[8] investigated further

$$Fe^{2+}{}_{aq} + H_2O_2 \rightarrow Fe^{3+}{}_{aq} + HO^\bullet + HO^- \qquad (1.1)$$

the mechanism of the Fenton reaction and proposed a second-order kinetic model, whereas, more than two decades later, Walling[3c] presented further evidence of the involvement of hydroxyl radicals in the oxidation of various organic compounds by the Fenton reagent.

However, recent thermodynamic calculations have demonstrated that an outer-sphere electron-transfer reaction between $Fe^{2+}{}_{aq}$ and H_2O_2, as it is rationalized by the classic mechanism proposed by Haber and Weiss (reaction 1.1), cannot take place, because the formation of the intermediate $H_2O_2{}^-$ is not favored.[9] In contrast, the formation of a hydrated iron(II)−H_2O_2 complex is thermodynamically favored. This reaction consists of a ligand exchange reaction (H_2O_2 vs H_2O) in the first ligand sphere of the iron(II) cation. For reasons of simplicity, we utilize for $Fe^{2+}{}_{aq}$ in reaction 1.2 the monomeric complex $[Fe(OH)(H_2O)_5]^+$

$$[Fe(OH)(H_2O)_5]^+ + H_2O_2 \underset{}{\overset{k \approx 2 \times 10^6\ s^{-1}}{\rightleftharpoons}} [Fe(OH)(H_2O_2)(H_2O)_4]^+ + H_2O \qquad (1.2)$$

instead of $[(H_2O)_4Fe(OH)_2Fe(H_2O)_4]^{2+}$, which may prevail depending upon the reaction conditions. By this exchange mechanism, a steady-state concentration of iron(II) bound to H_2O_2 is reached.

Note the remarkable difference between the monomolecular rate constant of ligand exchange in high-spin iron(II) complexes ($2 \times 10^6\ s^{-1}$)[10] and the bimolecular rate constant of the thermal Fenton reaction ($60-80\ M^{-1}\ s^{-1}$).[4d] From that comparison, it is clear that the formation of the key intermediate of the thermal Fenton reaction is not diffusion controlled as would be expected for an outer-sphere electron-transfer reaction.[9] In fact, an inner-sphere two-electron-transfer reaction slowly takes place within $[Fe(OH)(H_2O_2)(H_2O)_4]^+$ and the intermediate iron(IV) complex, $Fe^{4+}{}_{aq}$ ($[Fe(OH)_3(H_2O)_4]^+$), is formed (reaction 1.3).

$$[Fe(OH)(H_2O_2)(H_2O)_4]^+ \rightarrow [Fe(OH)_3(H_2O)_4]^+ \qquad (1.3)$$

Indeed, the existence of unusually charged metal complexes $Fe^{4+}{}_{aq}$, as well as $Fe^{5+}{}_{aq}$ and $Fe^{6+}{}_{aq}$, has been proven by stopped-flow experiments in combination with UV/vis absorption spectroscopy,[11] by chemical analysis of products formed during the Fenton oxidation,[12] and by pulse radiolysis of $Fe^{3+}{}_{aq}$[13] in the presence of inorganic ligands (HO^- and $P_2O_7{}^{4-}$). Furthermore, in the absence of H_2O_2 as reducing agent for highly charged iron cations, $Fe^{4+}{}_{aq}$ and $Fe^{6+}{}_{aq}$ possess surprisingly long lifetimes. The decays observed for both species in aqueous solution at pH 3−7 follow first-order kinetics with rate constants of approximately $2\ s^{-1}$.[14]

The intermediate iron(IV) complex ($Fe^{4+}{}_{aq}$) may react further leading to the formation of a free hydroxyl radical and $Fe^{3+}{}_{aq}$ ($[Fe(OH)(H_2O)_5]^{2+}$), as shown in reaction 1.4.

$$[Fe(OH)_3(H_2O)_4]^+ + H_2O \rightarrow [Fe(OH)(H_2O)_5]^{2+} + HO^\bullet + HO^- \qquad (1.4)$$

* To whom correspondence should be addressed.

S1089-5639(98)00129-7 CCC: $15.00
Published on Web 04/17/1998

SCHEME 1: Mechanistic Presentation of Possible Reactions Involved in the Thermal Fenton Reaction with Simplified Notations Used for the Various Iron Complexes)

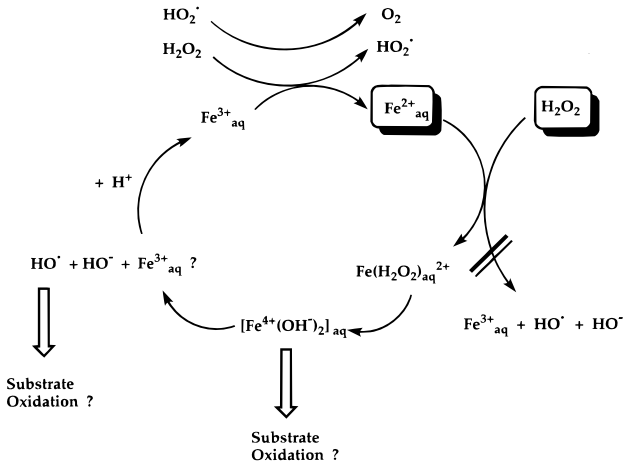

TABLE 1: Reduction Potentials of Fe^{2+}_{aq}, Fe^{3+}_{aq}, H_2O_2, and the Reactive Intermediates HO• and Fe^{4+}_{aq}

redox couple	E^0 (V vs NHE)
$HO^{\bullet}_{aq}/H_2O_{aq}$	2.59 (pH = 0)[a]
$HO^{\bullet}_{aq}/HO^{-}_{aq}$	1.64 (pH = 14)[a]
$Fe^{3+}_{aq}/Fe{=}O^{2+}$ (porphyrine chelate)	≈0.9 (pH = 0) [b]
$Fe^{3+}_{aq}/Fe{=}O^{2+}$ (porphyrine chelate)	≈1.3 (pH = 7) [b]
$Fe^{3+}_{aq}/Fe^{4+}_{aq}$	≈1.8 (pH = 0) [b]
$Fe^{3+}_{aq}/Fe^{4+}_{aq}$	≈1.4 (pH = 7) [b]
$Fe^{2+}_{aq}/Fe^{3+}_{aq}$	0.771 (pH = 0−3) [b]
H_2O_2/H_2O	1.776 (pH = 0)[a]
H_2O_2/H_2O	0.878 (pH = 14)[a]
H_2O_2/O_2	0.682 (pH = 0)[a]
H_2O_2/O_2	−0.076 (pH = 14)[a]

[a] Reference 19. [b] References 16−18.

Reaction pathways which may be of importance for the understanding of the mechanism of the Fenton reaction are shown in Scheme 1, which has been adapted from ref 15.

Although until recently it was a widely accepted paradigm in the field of AOP research that oxidations using the Fenton or the photochemically enhanced Fenton reactions are initiated by free hydroxyl radicals,[4−6] the question actually arises whether HO• production (reaction 1.4) is not too slow to compete with direct electron transfer between the substrate and an hydrated higher-valent iron species (most likely Fe^{4+}_{aq}). The reduction potentials of the reactive intermediates (HO•, Fe^{4+}_{aq}), as well as Fe^{2+}_{aq}, Fe^{3+}_{aq}, and H_2O_2, are listed in Table 1.[16−19]

Depending on the substrate, reactive intermediates other than the hydroxyl radical have been proposed for the Fenton reaction. In the case of compounds which may form highly stabilized iron(II) complexes[25] (e.g. EDTA), Sawyer et al.[20] suggested that the base-induced nucleophilic addition of H_2O_2 to the electrophilic iron center of these complexes yields the reactive intermediate of Fenton reagents.

One of the aims of this work was then to provide new experimental evidence for the involvement of hydrated higher-valent iron species as key intermediates of both thermal and photochemically enhanced Fenton reactions. 2,4-Xylidine (2,4-dimethylaniline) was chosen as the organic substrate, based on the fact that different reaction products should be formed depending on the reactive intermediates involved. Indeed, hydroxyl radicals react with organic compounds by addition to double bonds possessing a sufficient electron density, by hydrogen abstraction from alkyl groups or hydroxyl groups

SCHEME 2: Possible Reaction Pathways Involving Hydroxyl Radicals, Metal Cations and Organic Substrates in Aqueous Solution

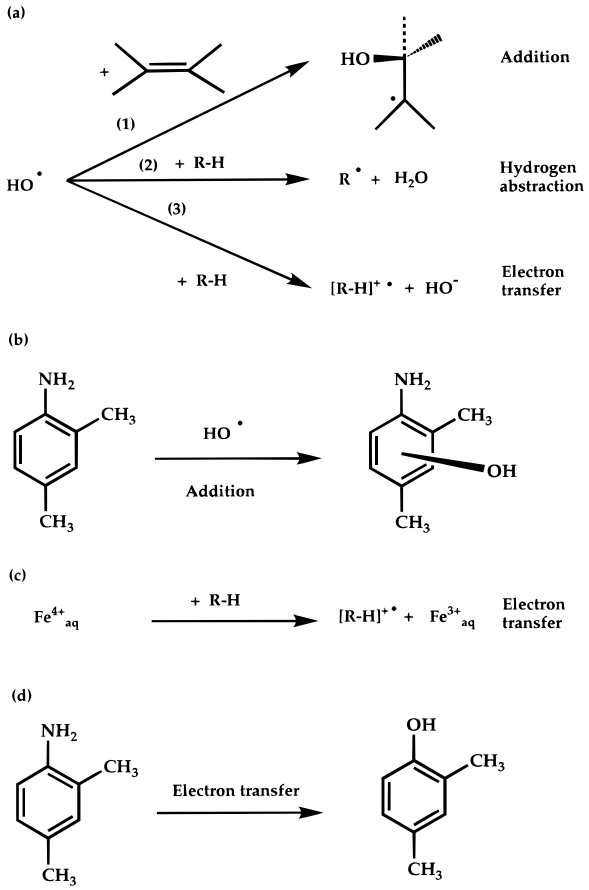

(albeit with lower efficiency), or by electron transfer (Scheme 2a).[19] Therefore, aminophenols should be generated during the reaction of 2,4-xylidine with hydroxyl radicals (Scheme 2b). The concentration of these products may strongly depend on the reaction conditions and on the irradiation times, but their presence would support a hydroxyl radical mechanism.

In contrast, the reaction of a metal cation, as for instance Fe^{4+}_{aq}, with an aliphatic or an aromatic hydrocarbon proceeds exclusively by an electron-transfer mechanism[21] (Scheme 2c), because neither addition nor hydrogen abstraction is possible. Under these conditions, the oxidation of 2,4-xylidine should not lead to the formation of aminophenols.

A second topic of this investigation concerns the mechanism of the photochemically enhanced recycling of Fe^{2+}_{aq}. Indeed, it has been shown recently that UV/visible irradiation accelerates both Fenton (H_2O_2/iron(II)) and Fenton-like (H_2O_2/iron(III)) reactions, improving the degradation rates of various organic contaminants.[5]

The reduction of Fe^{3+}_{aq} to Fe^{2+}_{aq} by H_2O_2 during the thermal Fenton reaction proceeds in three consecutive steps.[4] The first step consists of the formation of an hydrated iron(III)−H_2O_2 complex ($[Fe(OH)(HO_2)(H_2O)_4]^+$ at pH 3, reaction 2.1). An

$$[Fe(OH)(H_2O)_5]^+ + H_2O_2 \rightleftharpoons [Fe(OH)(HO_2)(H_2O)_4]^+ + H_3O^+ \quad (2.1)$$

inner-sphere electron-transfer reaction then occurs in the iron(III)−H_2O_2 complex, and iron(III) is reduced to iron(II) (reaction 2.2). A diffusion-controlled outer-sphere electron-transfer reaction then occurs between a second Fe^{3+}_{aq} complex

$$[Fe(OH)(HO_2)(H_2O)_4]^+ + H_2O \rightleftharpoons [Fe(OH)(H_2O)_5]^+ + HO_2^\bullet \quad (2.2)$$

($[Fe(OH)(H_2O)_5]^{2+}$) and the hydroperoxyl radical ($HO_2^\bullet$) formed in reaction 2.2, thus regenerating Fe^{2+}_{aq} (reaction 2.3). The

$$[Fe(OH)(H_2O)_5]^{2+} + H_2O + HO_2^\bullet \rightarrow [Fe(OH)(H_2O)_5]^+ + O_2 + H_3O^+ \quad (2.3)$$

reaction rate constants for the equilibrium reactions 2.1 and 2.2 are $k_{(2.1)} = 0.020\ M^{-1}\ s^{-1}$ and $k_{-(2.1)} = 1.2 \times 10^6\ M^{-1}\ s^{-1}$.[22] Reaction 2.3 is irreversible ($k_{(2.3)} = 2.88 \times 10^4\ M^{-1}\ s^{-1}$), and therefore the reaction sequence is shifted toward the thermal reduction of Fe^{3+}_{aq} to Fe^{2+}_{aq} and the corresponding oxidation of H_2O_2 to O_2. The enhancement of the reaction rate of iron(III) reduction under irradiation might be due to a photoinduced oxidation (by an inner-sphere electron-transfer reaction) of the ligands of various iron(III) complexes (with H_2O,[5f,g,23] with the organic substrate, or with its intermediates of degradation[5h,24]). The efficiency and the rate constants of the reduction of Fe^{3+}_{aq} to Fe^{2+}_{aq} are of particular importance for the optimization of the photochemically enhanced Fenton reaction. In this publication, we report values of the quantum yields for the photoreduction of iron(III) to iron(II) in aqueous solution in the absence and in the presence of oxalic acid or 2,4-xylidine. It is of special interest whether the quantum yields reported for the ferrioxalate actinometry,[26] where oxalate serves as ligand for iron(III) ($\Phi = 1.24$ at $\lambda = 254$ nm) are unique or whether aromatic amines (and other classes of organic compounds) react with similar quantum yields.

Experimental Section

Chemicals. $FeSO_4 \cdot 7H_2O Fe_2(SO_4)_2 \cdot 11H_2O$, H_2O_2, H_2SO_4, Na_3PO_4, $KMnO_4$, Na_2SO_3, KI, oxalic acid, 1,10-phenanthroline, and acetic acid were purchased from Merck. 2,4-Xylidine, 2,4-dimethylphenol, and 3-hydroxy-2,4-dimethylaniline were bought from Aldrich. Water was of bidistilled quality (UHQ II). All chemicals were ACS grade, except KNO_3 (Sigma), which was ultrapure.

UV/vis spectra were recorded using an Hewlett-Packard 5800(II) diode-array spectrophotometer. A Metrohm pH analyzer was employed (E 512). H_2O_2 was analyzed by classic $KMnO_4$ titration.[25]

DPP Spectra. All electrochemical experiments were performed with a computer-interfaced potentiostat/galvanostat (Princeton Applied Research, model 263A and software 270) using a conventional one-compartment cell and three-electrode configuration. The redox potentials were determined from differential pulse voltammetric (DPV) data. The setting of the pulse amplitude was 50 mV, the scan rate was 5 mV s^{-1}, and a glassy carbon electrode (3 mm diameter) was used as the working electrode. Unless otherwise indicated, the electrode potentials were referenced to the SHE. Before each experiment, the electrolyte solutions were purged with argon.

GC-MS/FTIR Analysis. For the qualitative and quantitative analysis of the reaction products generated during the H_2O_2 photolysis and the thermal and the photochemically enhanced Fenton reactions, the samples (2 mL) were injected into a GC (HP 5971A MSD, mass selective detector), coupled with a HP 5965B ID (infrared detector). A HP-INNOWAX capillary column (cross-linked poly(ethylene glycol)) was employed. All reaction products were identified by a combination of MS and FTIR spectroscopy in comparison with analytical data available from databases (MS, Wiley, Reference Mass Spectra, 1990; FTIR, EPA, Reference FTIR Spectra, 1992). For the structural determination of the reaction products, samples of 2,4-xylidine, 2,4-dimethylphenol, 3-hydroxy-2,4-dimethylaniline, and oxalic acid were co-injected (dissolved in $CHCl_3$), and in all cases, a superimposition of the corresponding peaks was observed. Furthermore, calibration curves for the compounds listed above were recorded. The results for all calibration samples could be fit to linear calibration curves.

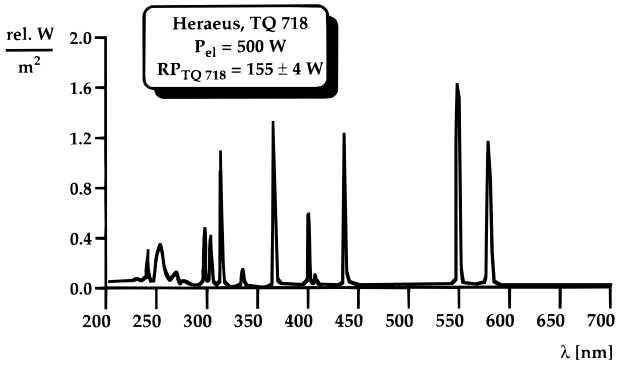

Figure 1. Relative spectral distribution of the medium-pressure mercury lamp (Heraeus, TQ 718) used for polychromatic irradiation experiments.

Ferrioxalate Actinometry. The radiant power [RP (W)] emitted by the medium-pressure mercury lamp (Heraeus, TQ 718, quartz filter, electrical power consumption 500 W) employed in all photochemical experiments described here was determined by using ferrioxalate actinometry[26] (Fe^{3+}_{aq}, 2.40×10^{-2} M; oxalic acid, 2.40×10^{-2} M). The method is based on the photochemical reduction of iron(III) to iron(II) during photooxidation of oxalic acid to CO_2 (see Results and Discussion). The photochemically generated Fe^{2+}_{aq} was measured quantitatively by using the UV/vis absorption of tris(1,10-phenanthroline)iron(II) ($[Fe(phen)_3]^{2+}$: $\epsilon_{(510\ nm)} = 11\ 100\ M^{-1}\ cm^{-1}$), which is formed from Fe^{2+}_{aq} and 1,10-phenanthroline in 0.50 M acetic acid.[26] Note that the solutions were diluted by a factor of 8 before taking UV/vis measurements in 1 cm quartz cells in order to ensure complete solubility of $[Fe(phen)_3]^{2+}$. Under the experimental standard conditions of the ferrioxalate actinometry, 9.37×10^{-5} M s^{-1} of Fe^{2+}_{aq} was formed. The incident radiations between 220 and 600 nm were absorbed by the chemical actinometer. From this quantitative data and using the relative emission spectrum of the lamp TQ 718, which is shown in Figure 1, the value for the radiant power emitted by the lamp (RP = 155 ± 4.0 W) was calculated according to eq 3.1, where $n(Fe^{2+})$ is the number of Fe^{2+}_{aq} ions formed during

$$RP = \frac{n(Fe^{2+})}{t\sum\left[\frac{S_{e,\lambda}}{E_{ph,\lambda}}(1 - 10^{-A_\lambda})\Phi_\lambda\right]} \quad (3.1)$$

the irradiation time (t in s), $S_{e,\lambda}$ is the relative spectral distribution of the radiant power emitted by the lamp (Figure 1), $E_{ph,\lambda}$ is the energy of a photon of wavelength λ (in J), A_λ is the average absorbance of the actinometric solution at wavelength λ during irradiation, and Φ_λ is the quantum yield of the chemical actinometer at wavelength λ.[26]

As it becomes clear from eq 3.1, the measurement has been performed under polychromatic integration. The wavelength dependence of the quantum yield of the photoreduction of ferrioxalate and the relative photonic emission of the mercury medium-pressure lamp have been integrated. For the photolysis

TABLE 2: Rates of Photons Absorbed (P_a) by the Iron(III) Complexes in Solution (pH 3.0; Radiant Power of the TQ 718 Lamp, RP = 155 ± 4.0 W)

photolyzed system (pH = 3)	P_a (einstein L^{-1} s^{-1})[a]
Fe^{3+}_{aq}, 2.40×10^{-2} M; oxalic acid, 2.40×10^{-2} M	8.23×10^{-5}
Fe^{3+}_{aq}, 6.50×10^{-4} M; oxalic acid, 2.08×10^{-2} M	3.32×10^{-5}
Fe^{3+}_{aq}, 6.50×10^{-4} M; 2,4-xylidine, 5.20×10^{-3} M	3.30×10^{-5}
Fe^{3+}_{aq}, 6.50×10^{-4} M; H_2O_2, 5.41×10^{-2} M	3.39×10^{-5}
Fe^{3+}_{aq}, 6.50×10^{-4} M; H_2O, 55.51 M	3.26×10^{-5}

[a] The standard deviation (from 3 experiments) did not exceed ±5 relative %.

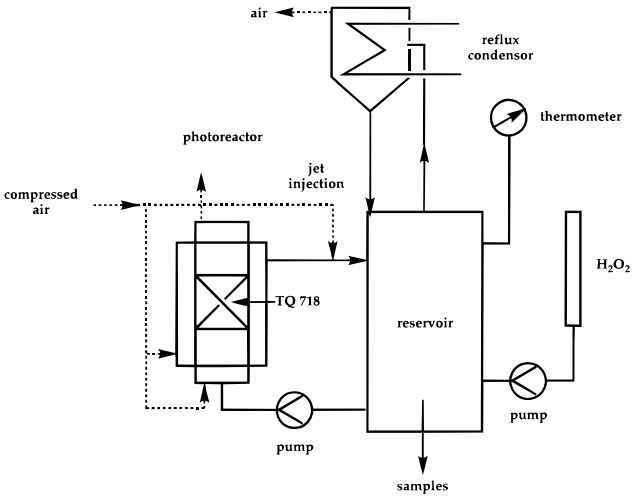

Figure 2. Photochemical pilot reactor employed in all irradiation experiments (reservoir, $V = 2.0$ L; photochemical reactor, $V = 1.25$ L; optical path length = 2 cm; diameter = 11 cm; cutoff of the quartz sleeve, 220 nm).

systems investigated here, the radiant power which is absorbed by the photolyzed solution is distinctly lower, because a lower concentration of Fe^{3+}_{aq} (6.50×10^{-4} M) was chosen, according to the conditions employed in pilot scale reactors for photochemically enhanced Fenton oxidation.[5,6] Therefore, the rate of photons absorbed (P_a) by the iron(III) complexes in various solutions has been included in Table 2. The values P_a (in Einstein L^{-1} s^{-1}) have been calculated according to eq 3.2,

$$P_a = \sum_\lambda P_{a,\lambda} = \frac{RP}{VN_A} \sum_\lambda \left[\frac{S_{e,\lambda}}{E_{ph,\lambda}} (1 - 10^{-A_\lambda}) \right] \qquad (3.2)$$

where $P_{a,\lambda}$ is the rate of photons absorbed at wavelength λ (wavelength range: 220−600 nm), N_A the Avogadro number, and V the total volume of the solution in L.

Since the emission spectrum of the mercury medium-pressure lamp is well resolved, and the dependence of the quantum yield of the ferrioxalate actinometer on the absorbed wavelength is well-known,[26] P_a can be calculated easily in this particular case.

DOC Analyzer. The analyses of the DOC (dissolved organic carbon) were carried out using a Dohrmann DC-190 TOC (total organic carbon) analyzer (T = 680 °C) from Rosemount Analytical. Calibrations were performed using 2,4-xylidine, oxalic acid, and potassium hydrophthalate (KHP). The results for all calibration samples could be fitted with linear calibration curves.

H_2O_2 Photolysis. All photolysis experiments were carried out in a pilot reactor shown in Figure 2. It consists of a reservoir ($V = 2.0$ L) and a flow-through annular photoreactor, equipped with a TQ 718 medium-pressure mercury lamp. The solution was pumped (10 ± 1 L min^{-1}) by means of a MPN 80 pump (Schmitt-Kreiselpumpen) under continuous jet-injection of compressed air. The photolysis experiments were performed during 120 min. The starting temperature was 25 ± 2 °C. During the first 20 min, a linear increase of the reaction temperature was observed. After this initial time period, the temperature remained constant at 60 ± 3 °C.

The total volume of the photolysis solution was 2.50 L (2,4-xylidine, 500 mg of C L^{-1} (500 ppm C), 5.41×10^{-3} M; H_2O_2, 5.41×10^{-2} M). The pH was adjusted to the initial value of 3.0 using H_2SO_4. The analysis was performed immediately after taking the samples, which were filtered using Nylon Luer-Lock membrane filters (Roth, 0.22×10^{-6} m). The filtered solution was extracted with $CHCl_3$ (10 mL of photolysis solution + 1 mL of $CHCl_3$). Since numerous reaction products appeared in the GC-MS/FTIR traces, only reaction products formed at concentrations higher than 10^{-6} M were identified.

Thermal and Photochemically Enhanced Fenton Reactions and Control Experiment. The Fenton oxidation experiments, as well as the irradiation of 2,4-xylidine at pH 3.0 in the absence of additional chemicals, were carried out in the pilot reactor already described (Figure 2). The concentration of 2,4-xylidine was 500 mg of C L^{-1}, 5.41×10^{-3} M. During the first 120 min of irradiation time, H_2O_2 was continuously added (2.25×10^{-3} mol min^{-1}, 0.2705 mol of H_2O_2 in 0.10 L in total). In both Fenton reactions, $FeSO_4 \cdot 7H_2O$ (6.50×10^{-4} M) was dissolved in the presence of 2,4-xylidine. Again, the pH was adjusted to the initial value of 3.0 by adding H_2SO_4. The irradiation was continued for an additional time period of 60 min in order to complete the degradation reactions or to reach a plateau region, respectively. A control experiment was carried out by irradiating 2,4-xylidine at pH 3.0 in the absence of additives.

Treatment of the Samples Prior to $CHCl_3$ Extraction and HPLC Injection. A 2.0×10^{-3} L volume of "reduction and precipitation agent" (composed of 0.10 M Na_3PO_4, 0.10 M KI, and 0.10 M Na_2SO_3) was added to a volume of 5.0×10^{-3} L taken from the pilot reactor at different times. This procedure led to a complete reduction of the residual H_2O_2 as well as to the removal of most of the iron(II/III). The precipitate was removed by filtration using the Nylon filters (Roth) already described. After this procedure, the solutions were extracted with $CHCl_3$ and injected into the GC-MS/FTIR spectrometer.

Results and Discussion

Electrochemical Results. The electrochemical properties of 2,4-xylidine have been investigated by employing differential pulse voltammography (DPP). 2,4-Xylidine, dissolved in water, possesses two distinct oxidation waves between pH 6 and pH 3 (Figure 3). At the latter pH, which was chosen for all AOP experiments described here, two distinct oxidation waves at 0.670 and 0.760 V (vs SHE) are discernible.

This result can be rationalized by the equilibrium of the free and the protonated aromatic amine.[27] At pH < 3 only one oxidation wave was obtained due to complete protonation of 2,4-xylidine. Note that both the hydroxyl radical ($E = 2.38$ V at pH 3.0) and the ferryl ion (Fe^{4+}_{aq}: $E \approx 1.65$ V at pH 3.0) possess a sufficiently high oxidation potential for the oxidation of 2,4-xylidine (Table 1). Whereas Fe^{3+}_{aq} ($E = 0.66$ V at pH 3.0) does not oxidize 2,4-xylidine in the dark, the electronically excited cation Fe^{3+*}_{aq} ($E \approx 2.43$ V at pH 3.0)[28] is a strong oxidant, and therefore, it is capable of oxidizing 2,4-xylidine when coordinated in iron(III) complexes.

On the basis of the electrochemical literature,[27] two reaction pathways for oxidation/reduction sequences of aromatic amines

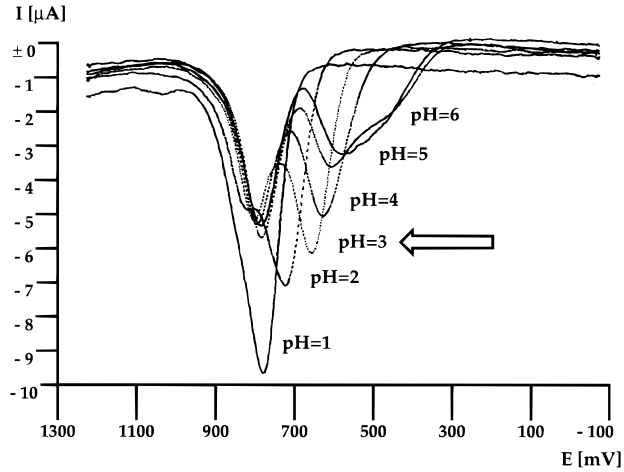

Figure 3. Electrochemical characterization of the redox properties of 2,4-xylidine by differential pulse voltammography: 125 mg of C L^{-1} of 2,4-xylidine in 0.10 M KNO_3 in aqueous solution, helium atmosphere.

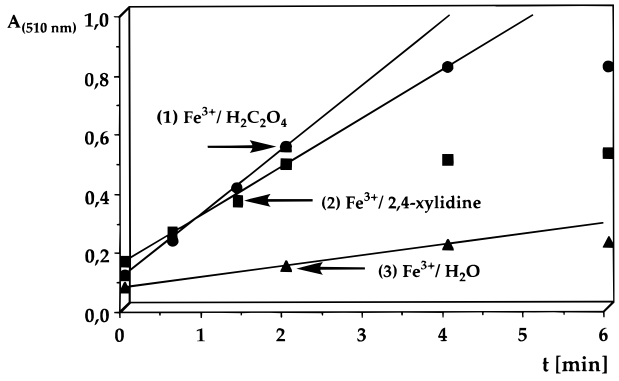

Figure 4. Fe^{2+}_{aq} formation monitored by the increase of the absorbance of the $[Fe(phen)_3]^{2+}$ complex [$A_{(510\ nm)}$] as a function of irradiation time (lamp: TQ 718; RP = 155 ± 4 W). The solutions have been purged with N_2 for 15 min prior to photolysis. Key: (1) $[Fe^{3+}_{aq}] = 6.50 \times 10^{-4}$ M, [oxalic acid] $= 2.08 \times 10^{-2}$ M, pH 3.0, plateau value corresponds to 100% reduction of iron(III) to iron(II); (2) $[Fe^{3+}_{aq}] = 6.50 \times 10^{-4}$ M, [2,4-xylidine] $= 5.41 \times 10^{-3}$ M, pH 3.0, plateau value corresponds to 63% reduction of iron(III) to iron(II); (3) $[Fe^{3+}_{aq}] = 6.50 \times 10^{-4}$ M, $[H_2O] = 55.5$ M, pH 3.0, plateau value corresponds to 32% reduction of iron(III) to iron(II).

according to electron-transfer mechanisms can be proposed. Whereas the oxidation of aromatic amines at the anode usually leads to the formation of nitro compounds, the combination of oxidation and reduction conditions can open pathways for the formation of phenols. In Scheme 3, two reaction pathways for the formation of phenols are proposed. In both cases, the initial step consists of an electron-transfer reaction from 2,4-xylidine to Fe^{4+}_{aq} and leads to the formation of Fe^{3+}_{aq} and an aromatic cation radical [2,4-xylidine]$^{+\bullet}$. The exchange of the amine group of this reactive intermediate versus water is possible. At pH 3, the ammonium cation can leave the molecule and the aromatic phenol cation radical [2,4-dimethylphenol]$^{+\bullet}$ can be formed. Finally, in a third step, 2,4-dimethylphenol can be created via an electron-transfer reaction. In principle, Fe^{2+}_{aq}, H_2O_2 (see Table 1), and various organic radicals may serve as electron donors under the experimental conditions of the Fenton reactions. This reaction branch can be labeled an oxidation/aromatic substitution/reduction (O_x-S_Ear-Red)-mechanism. The second step of the alternative reaction pathway consists of an electron-transfer oxidation of [2,4-dimethylxylidine]$^{+\bullet}$. In this case, the aromatic amine group of 2,4-xylidine leaves as hydroxylamine and again 2,4-dimethylphenol can be formed. This reaction pathway can be labeled as an oxidation/aromatic substitution/oxidation ($O_x-S_Ear-O_x$) mechanism.

Determination of the Quantum Yields of Several Model Reactions for the Photochemical Reduction of Iron(III) to Iron(II). As already discussed in the Introduction, the design of efficient AOP reactors which rely on the photochemically enhanced Fenton reaction depends strongly on the knowledge of fundamental data, such as the quantum yields of the Fe^{3+}_{aq} reduction and the chemical nature of the key intermediate. Therefore, we have compared (in the pilot reactor already described (Figure 2)) the ferrioxalate photoreaction with the reduction of iron(III) in the presence and in the absence of 2,4-xylidine under polychromatic irradiation (Experimental Section and Figure 4). In all cases, the pH of the photolyzed solutions

SCHEME 3: Proposed Reaction Pathways for the Oxidation/Reduction of 2,4-Xylidine via Electron Transfer Reactions[a]

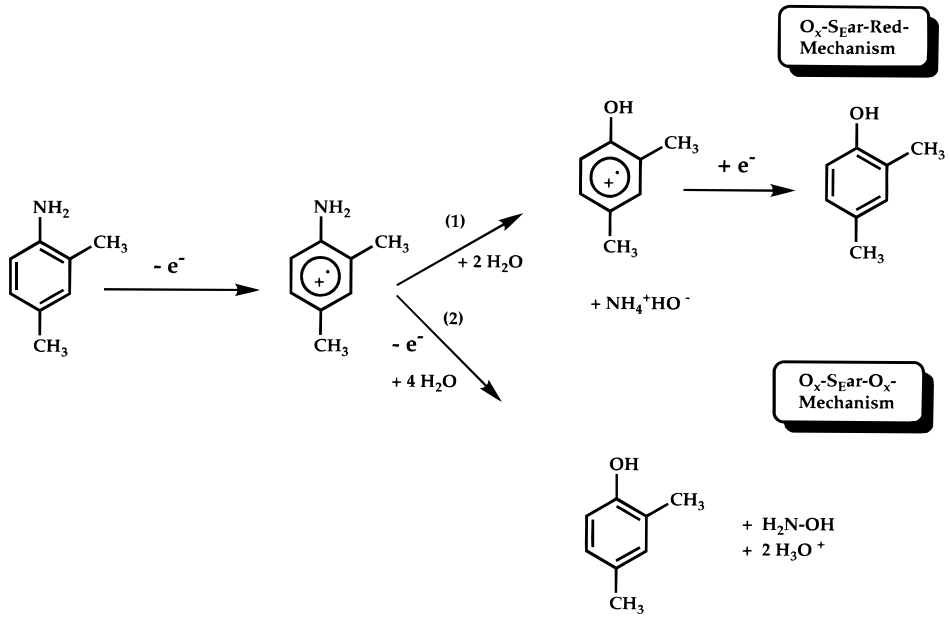

[a] Two different reaction pathways are possible: (1) oxidation/aromatic substitution/reduction (O_x-S_EAr-Red) mechanism; (2) oxidation/aromatic substitution/oxidation ($O_x-S_EAr-O_x$) mechanism.

TABLE 3: Initial Rate Constants (k) and Quantum Yields of Iron(II) Formation under Polychromatic Irradiation ($\langle\Phi(\mathrm{Fe(II)})\rangle$) in Model Systems of the Photochemically Enhanced Fenton Reaction (Corresponding Values for Hydrogen Peroxide Photolysis Also Indicated) (Standard Deviation: ±3%)

photolyzed system	c(Fe(III)) (M)	c(substrate) (M)	10^5k(Fe(II)) (M s^{-1})	$\langle\Phi(\mathrm{Fe(II)})\rangle$ (lamp TQ 718)
$Fe^{3+}/H_2C_2O_4$	2.40×10^{-2}	2.40×10^{-2}	9.38	1.14[a]
$Fe^{3+}/H_2C_2O_4$	6.50×10^{-4}	2.08×10^{-2}	6.48	1.21
Fe^{3+}/H_2O	6.50×10^{-4}	55.5	1.08	0.21
Fe^{3+}/2,4-xylidine	6.50×10^{-4}	5.20×10^{-3}	4.92	0.92

photolyzed system	c(Fe(III)) (M)	c(substrate) (M)	$-10^5k(H_2O_2)$ (M s^{-1}) $\times 10^5$	$\langle\Phi(\mathrm{Fe(II)})\rangle$
Fe^{3+}/H_2O_2 [c]	6.50×10^{-4}	2.40×10^{-2}	7.07	≈0.33 (1.32[b])

photolyzed system	c(Fe(III)) (M)	c(substrate) (M)	$-10^5k(H_2O_2)$ (M s^{-1})	$\langle\Phi(HO^•)\rangle$
H_2O_2		6.50×10^{-3}	0.06	≈0.02

[a] Calculated using eqs 3.2 and 3.3, taking into account the relative emission spectrum of the medium-pressure mercury lamp (TQ 718; see Figure 1). This value has been used as a reference polychromatic quantum yield for the determination of the other quantum yields presented in Table 3. [b] Quantum yield of H_2O_2 consumption. [c] The second-order rate constant of the thermal H_2O_2 decomposition at 25 °C in the presence of $Fe^{3+}{}_{aq}$ was $k = 4.48\ (\pm 0.1) \times 10^{-3}$ M^{-1} s^{-1}.

has been adjusted exactly to 3.0 by means of H_2SO_4. The amount of iron(II) has been measured after formation of the $[Fe(phen)_3]^{2+}$ complex as described in the Experimental Section (Ferrioxalate Actinometry).

The "quantum yields" of iron(II) production under polychromatic irradiation $<\Phi(Fe^{2+})>$ by means of a medium-pressure Hg lamp (TQ 718) have been calculated according to the standard eq 3.3 used under monochromatic irradiation.[26]

$$\langle\Phi(Fe^{2+})\rangle = \frac{dn}{dt\,P_a} \tag{3.3}$$

$$P_a = \text{rate of photons absorbed (einstein L}^{-1}\text{ s}^{-1}\text{)}$$

$$dn/dt = \text{rate of Fe}^{2+}\text{ formation (M s}^{-1}\text{)}$$

As indicated in Table 3, the quantum yield determined for the reduction of $Fe^{3+}{}_{aq}$ by 2,4-xylidine is almost unity and hence surprisingly high. From this result, we may deduce that an organic compound, which is able to serve as a ligand in iron(III) complexes and possesses a suitable oxidation potential, can undergo an efficient inner-sphere electron transfer to electronically excited iron(III) leading to iron(II) formation. Furthermore, the quantum yield measured in this work for the photochemical oxidation of water by $Fe^{3+}{}_{aq}$* is at the upper limit of the data reported in the literature, which ranges from 0.065 [5c] to 0.24.[23c]

In the three cases shown in Figure 4 (oxalic acid, 2,4-xylidine, and H_2O as ligands for iron(III) photooxidation), plateau regions were reached at different iron(II) concentrations.

(1) The photolysis of $[Fe(C_2O_4)_3]^{3-}$ led to a complete reduction of iron(III) to iron(II) (100%, 6.50×10^{-4} M $Fe^{2+}{}_{aq}$) according to the established ferrioxalate reaction mechanism:[26]

$$[Fe(C_2O_4)_3]^{3-} \xrightarrow{h\nu} [Fe(C_2O_4)_2]^{2-} + C_2O_4^{\bullet-} \tag{4.1}$$

$$[Fe(C_2O_4)_3]^{3-} + C_2O_4^{\bullet-} \xrightarrow{h\nu} [Fe(C_2O_4)_2]^{2-} + C_2O_4^{2-} + 2CO_2 \tag{4.2}$$

SCHEME 4: Electron-Transfer Reaction between Electronically Excited Iron(III) and 2,4-Xylidine and Following Thermal Reaction Steps[a]

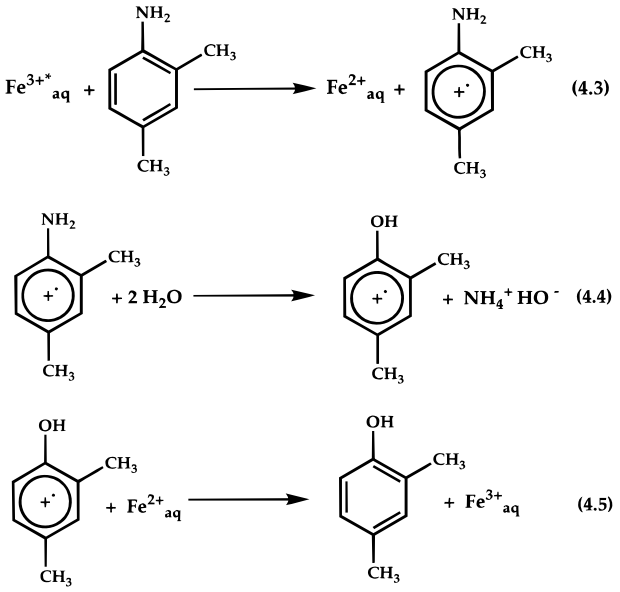

[a] Note that reaction 4.3 most likely proceeds within a hydrated Iron(III)−2,4-xylidine complex.

(2) In contrast to case (1), the oxidation of 2,4-xylidine by $Fe^{3+*}{}_{aq}$ led to a plateau region (≈ 4.1×10^{-4} M $Fe^{2+}{}_{aq}$) corresponding to a steady-state concentration of approximately 63% (Figure 4). Therefore, it can be concluded that at least one reaction pathway for the depletion of $Fe^{2+}{}_{aq}$ exists. The photoinduced redox reactions shown in Scheme 4 explain the observed reaction behavior.

The formation of 2,4-dimethylphenol was observed by GC-MS/FTIR. After 12 min of irradiation time, $6.0 \pm 0.5 \times 10^{-5}$ M of 2,4-dimethylphenol was detected. This experimental finding confirms that an oxidation/reduction pathway from 2,4-xylidine to 2,4-dimethylphenol exists.

(3) During the oxidation of water by $Fe^{3+}{}_{aq}$*, a plateau region (≈2.0×10^{-4} M $Fe^{2+}{}_{aq}$, corresponding to a steady-state concentration of approximately 32%, Figure 4) was observed. It is noteworthy that reaction 4.6 generates hydroxyl radicals.[5c,23]

$$Fe^{3+}{}_{aq} + H_2O \xrightarrow{h\nu} Fe^{2+}{}_{aq} + HO^• + H^+ \tag{4.6}$$

However, its quantum yield ($\langle\Phi(\mathrm{Fe(II)})\rangle = 0.21$) is significantly lower than that of the oxidation of oxalic acid ($\langle\Phi(\mathrm{Fe(II)})\rangle = 1.14$) or 2,4-xylidine ($\langle\Phi(\mathrm{Fe(II)})\rangle = 0.92$) (see Table 3), and therefore, under AOP conditions, the latter reactions will be dominant as long as organic compounds are present in solution and reaction 4.6 will be of minor importance.

Several mechanisms for the depletion of $Fe^{2+}{}_{aq}$ exist:[3c] (a) The back-reaction of (4.7) proceeds as diffusion controlled. (b)

$$Fe^{2+}{}_{aq} + OH^• + H^+ \rightarrow Fe^{3+}{}_{aq} + H_2O \tag{4.7}$$

The thermal Fenton reaction (reactions 1.2 and 1.3) also takes place, leading to a depletion of both $Fe^{2+}{}_{aq}$ and H_2O_2. (c) The ferryl ion ($Fe^{4+}{}_{aq}$) generated in the thermal Fenton reaction 1.3 is able to react with $Fe^{2+}{}_{aq}$ (reaction 4.8). A reaction rate

$$Fe^{4+}{}_{aq} + Fe^{2+}{}_{aq} \rightarrow 2Fe^{3+}{}_{aq} \tag{4.8}$$

constant for this process could not be found in the literature. However, Walling already published in 1975 that the back-

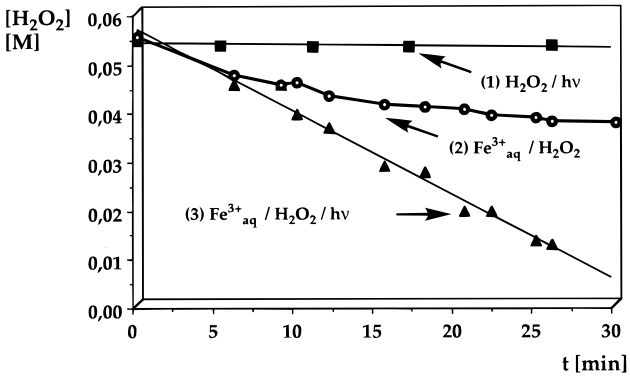

Figure 5. H_2O_2 concentration as a function of irradiation time (lamp: TQ 718) in the following systems: (1) $[H_2O_2] = 5.41 \times 10^{-2}$ M, TQ 718 irradiation (□) (2) $[Fe^{3+}] = 6.50 \times 10^{-4}$ M, $[H_2O_2] = 5.41 \times 10^{-2}$ M, dark reaction (○) (3) $[Fe^{3+}] = 6.50 \times 10^{-4}$ M, $[H_2O_2] = 5.41 \times 10^{-2}$ M, TQ 718 irradiation (▲).

reaction of the thermal Fenton reaction proceeds diffusion controlled.[3c] In the classic mechanistic interpretation, the formation of the hydroxyl radical as intermediate was postulated. However, if the ferryl ion and not the hydroxyl radical is the key intermediate of the thermal Fenton reaction, the measured rate constant remains unchanged!

(4) Since H_2O_2/HO_2^- is competing with water and coordinating organic molecules as a ligand in hydrated iron(III) complexes, the quantum yield of the photooxidation of H_2O_2 in aqueous solution in the presence of iron(III) is of importance for the mechanistic understanding of the photochemically enhanced Fenton reaction. The analysis of Fe^{2+}_{aq} formed during irradiation in analogy to the classic ferrioxalate reaction (*vide supra*) could not be performed, because Fe^{2+}_{aq} quickly reacts with H_2O_2 (thermal Fenton reaction). We have therefore followed the consumption of H_2O_2 during irradiation. As it can be seen in Figure 5 (case (3)), a linear dependence of the H_2O_2 concentration has been obtained (photochemical reaction of pseudo-zero-order). This is typically observed if a photoinitiated inner-sphere electron-transfer reaction takes place. Thus, the photoenhancement of the reduction of iron(III) by H_2O_2 may be the result of the absorption of a photon by the hydrated iron(III)$-H_2O_2$ complex $[Fe(OH)(HO_2)(H_2O)_4]^+$, followed by an inner-sphere electron transfer leading to the formation of $[Fe(OH)(H_2O)_5]^+$ (Fe^{2+}_{aq}) and the hydroperoxyl radical ($HO_2^\bullet$) (reaction 5.1). This process is faster than the reduction of iron(III) to iron(II) in the ground-state iron(III)$-H_2O_2$ complex (reaction 2.2).

$$[Fe(OH)(HO_2)(H_2O)_4]^{+}* + H_2O \rightarrow [Fe(OH)(H_2O)_5]^{+} + HO_2^\bullet \quad (5.1)$$

Furthermore, the quantum yield measured for the H_2O_2 disappearance is equal to 1.32. Therefore, the photoinduced H_2O_2 decomposition (reaction 5.1) cannot be neglected in a kinetic model of the photochemically enhanced Fenton reaction: this photochemical process is always competing with the oxidation of organic compounds by $Fe^{3+}*_{aq}$ (Scheme 4). Reaction 5.1 is followed by reaction 2.3 as in the thermal process, and a second Fe^{3+}_{aq} is thermally reduced to Fe^{2+}_{aq} by $HO_2^\bullet$. Fe^{2+}_{aq} produced in reactions 5.1 and 2.3 participates in the thermal Fenton reaction (reactions 1.2 and 1.3). Finally, the reactive intermediate formed in the latter reaction (Fe^{4+}_{aq}) oxidizes H_2O_2.[3c] As a consequence, a total of 4 molecules of H_2O_2 are consumed for each photon absorbed by $Fe^{3+}(HO_2^-)_{aq}$ ($[Fe(OH)(HO_2)(H_2O)_4]^+$). It follows that a quantum yield for

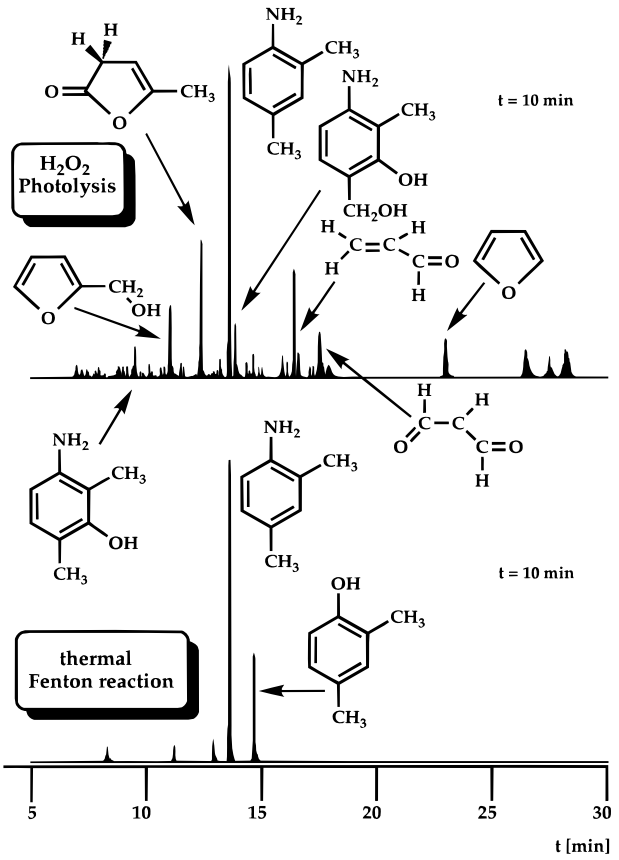

Figure 6. Comparison of the GC/MS traces of 2,4-xylidine and the reaction intermediates formed after 10 min of H_2O_2 photolysis and 10 min of the thermal Fenton reaction. (The peak of oxalic acid is not shown due to its interference with the $CHCl_3$ peak (solvent for extraction).)

the reduction of $Fe^{3+}(HO_2^-)_{aq}^*$ by H_2O_2 of $\langle\Phi(Fe(II))\rangle = 0.33$. It also can be seen from Figure 5 that the photolysis of H_2O_2 (without addition of Fe^{3+}_{aq}) can be neglected and that the thermal reduction of Fe^{3+}_{aq} to Fe^{2+}_{aq} by H_2O_2 ($k = (4.48 \pm 1) \times 10^{-3}$ M^{-1} s^{-1}) (Figure 5) is of minor importance.

2,4-Xylidine Oxidation Mechanisms Employing Hydrogen Peroxide Photolysis: Thermal and the Photochemically Enhanced Fenton Reactions. As already discussed in the Introduction, our experimental strategy for investigating the existence of the hydroxyl radical as key intermediate of both Fenton reactions consisted in the comparison of the reaction products of 2,4-xylidine generated by H_2O_2 photolysis with the intermediates created in both Fenton reactions.

It is well established that the UV photolysis of H_2O_2 leads to the formation of free hydroxyl radicals.[1,29]

$$H_2O_2 \xrightarrow{h\nu\ (UV)} 2HO^\bullet \quad (6.1)$$

Figure 6 and Table 4 show that entirely different intermediates are formed during H_2O_2 photolysis on one hand and both Fenton reactions on the other hand.

Before the results of the photochemical experiments performed in the pilot reactor are discussed, it should be noted that the photolysis of 2,4-xylidine at pH 3.0 did not lead to any detectable degradation products. To achieve a quantitative understanding of the AOP reactions investigated, the DOC (dissolved organic carbon) of the irradiated solutions has been measured using a catalytic DOC analyzer, and the intermediates have been identified and determined quantitatively by GC/MS.

TABLE 4: Reaction Intermediates Identified by MS and FTIR and Their GC Retention Times

compd	GC retention time (min)
H_2O_2 Photolysis	
3-hydroxy-2,4-dimethylaniline	8.75
furfuryl alcohol	11.82
2(3*H*)-5-methylfuranone	13.55
2,4-xylidine	14.10
4-amino-2-hydroxy-3-methylbenzyl alcohol	14.47
acroleine	16.86
malondialdehyde	17.62
furane	24.11
Thermal and Photochemically Enhanced Fenton Reaction	
oxalic acid	1.27
3,5-dimethyl-*o*-benzoquinone	2.71
2-hydroxy-5-methylbenzyl alcohol	4.37
2,4-xylidine	14.10
2,4-dimethylphenol	14.83

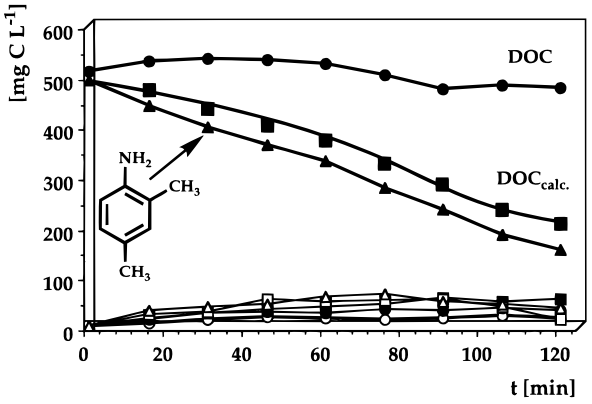

Figure 7. Photochemical oxidative degradation of 2,4-xylidine in the presence of H_2O_2 (initial 2,4-xylidine concentration, 5.41×10^{-3} M (500 mg of C L^{-1}); pH 3.0; initial H_2O_2 concentration, 5.41×10^{-2} M): 2,4-xylidine concentration (▲); measured DOC (●); calculated DOC (■); minor intermediates (other symbols).

The concentrations of the most important intermediates and of 2,4-xylidine have then been added (DOC_{calc}) and compared to the DOC measured experimentally.

In Figure 7, the results of the H_2O_2/UV treatment of a 2,4-xylidine aqueous solution are shown: the concentration of 2,4-xylidine decreases according to a pseudo-zero-order kinetic ($k = (1.18 \pm 0.05) \times 10^{-1}$ M s^{-1}). However, the DOC does not change during 120 min of irradiation within the limits of experimental error [±8 relative %]. Some of the intermediates are listed in Table 4. Figure 7 shows that a quantitative mass balance of this reaction could not be measured.

Figure 8 shows the results of 2,4-xylidine degradation by the thermal Fenton reaction. In agreement with the analytical results listed in Table 4, the chemistry of the thermal Fenton reaction is very different from the chemistry of the H_2O_2 photolysis. 2,4-Dimethylphenol is the main intermediate of the thermal Fenton degradation of 2,4-xylidine. This finding strongly supports the mechanistic hypothesis described in Scheme 4. Assuming a pseudo-first-order kinetic for the decomposition of 2,4-xylidine, a reaction rate constant $k = 6.59 \times 10^{-4}$ s^{-1} was obtained. Oxalic acid was found to be the main reaction product, and the loss of DOC was only approximately 150 mg of C L^{-1}. Further oxidation of oxalic acid was not observed. This finding can be explained by the high kinetic stability of the iron(III) tris(oxalate) complex, $[Fe(C_2O_4)_3]^{3-}$,[30] preventing the formation of hydrated iron(III)−H_2O_2 complexes and, thus, recycling of iron(III) to iron(II). An excellent agreement between calculated and measured DOC values was observed for the complete irradiation time.

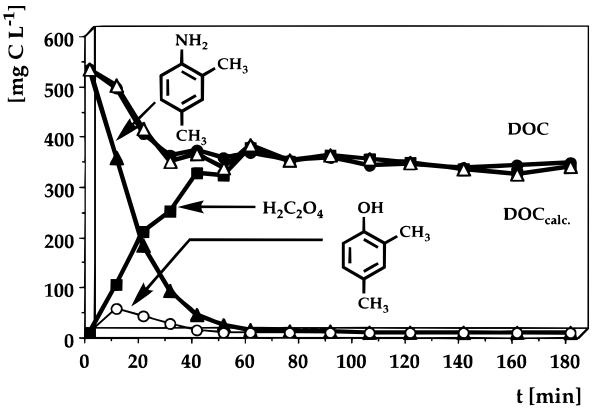

Figure 8. Thermal Fenton reaction of 2,4-xylidine (initial concentration: 5.41×10^{-3} M (500 mg of C L^{-1}); initial $FeSO_4 \cdot 7H_2O$ concentration, 6.50×10^{-4} M; pH 3.0; H_2O_2 added continuously (0.2705 mol in 0.10 L during 120 min): 2,4-xylidine (▲); 2,4-dimethylphenol (○), oxalic acid (■); calculated DOC (△); measured DOC (●).

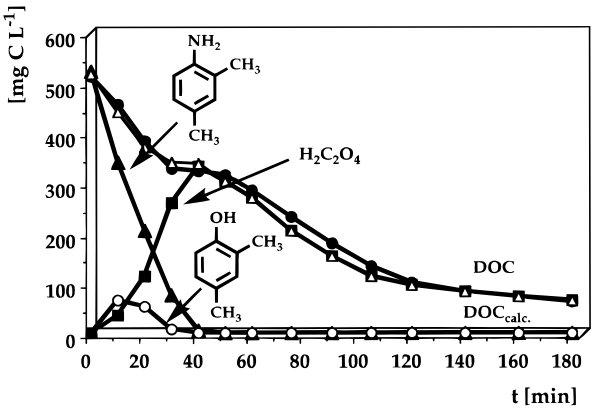

Figure 9. Photochemically enhanced Fenton reaction of 2,4-xylidine (initial concentration, 5.41×10^{-3} M (500 mg of C L^{-1}); initial $FeSO_4 \cdot 7H_2O$ concentration, 6.50×10^{-4} M; pH 3.0; H_2O_2 added continuously (0.2705 mol in 0.10 L during 120 min): 2,4-xylidine (▲); 2,4-dimethylphenol (○); oxalic acid (■); calculated DOC (△); measured DOC (●).

The comparison of Figures 8 and 9 shows that the photochemically enhanced Fenton reaction leads within an irradiation time of 120 min to an almost complete removal of the DOC. The complete decomposition of 2,4-xylidine was already achieved after 60 min of irradiation time. Assuming a pseudo-first-order kinetic, a reaction rate constant $k_1 = 6.61 \times 10^{-4}$ s^{-1} was calculated. After 35 min of irradiation, the decomposition rate of 2,4-xylidine increased and $k_2 = 2.3 \times 10^{-3}$ s^{-1} was found. We attribute this increase of the 2,4-xylidine decomposition rate to a decrease of inner filter effects (appearance of a purple-brown color), which was strongest at the earliest stages of the photolyses. The chemical nature of the main intermediates (>3 mg of C L^{-1}) was exactly the same as that of the thermal Fenton reaction, but their concentrations were lower. In this experiment also, the measured and the calculated DOC values were in very good agreement. The faster removal of DOC, which at later reaction times consisted mainly of oxalic acid, can be explained by the photodegradation of $[Fe(C_2O_4)_3]^{3-}$ (ferrioxalate reactions 4.1 and 4.2).

Conclusions

The products of 2,4-xylidine degradation during H_2O_2 photolysis and during the thermal and photochemically enhanced Fenton reactions have been analyzed using GC-MS/FTIR. Whereas general agreement exists in the literature that H_2O_2

TABLE 5: Summary of the Observed Reaction Behavior

reacn system (aq solutn)	electronic confign of iron(II/III)	reactive intermediate of the thermal reacn ($T = 295$ K)	reactive intermediate of the photochem reacn ($\lambda_{irr} = 200-550$ nm)
$Fe^{2+}_{aq} + H_2O_2$	high-spin $(t_{2g})^4(e_g)^2$	Fe^{4+}_{aq}	
Fe^{3+}_{aq}	high-spin $(t_{2g})^5(e_g)^0$		HO•

photolysis yields free hydroxyl radicals, a controversy about the reactive intermediates of the thermal and the photochemically enhanced Fenton reactions still prevails. The comparison of the reaction products of 2,4-xylidine clearly demonstrates that H_2O_2 photolysis on one hand and both Fenton reactions on the other hand involve different reactive intermediates. Whereas hydroxylated aromatic amines are formed during H_2O_2 photolysis, 2,4-dimethylphenol is the most important intermediate in both Fenton reactions. 2,4-Dimethylphenol can be formed by an electron-transfer mechanism. Therefore, we conclude that during the thermal reaction of Fe^{2+}_{aq} with H_2O_2 a cationic iron intermediate possessing an unusual charge, most likely the ferryl ion (Fe^{4+}_{aq}), is formed. However, the experiments described here cannot distinguish between Fe^{4+}_{aq} and a hydroxyl radical complexed by Fe^{3+}_{aq}. The latter species would possess exactly the same reactivity as Fe^{4+}_{aq}.

In contrast to the thermal Fenton reaction, evidence for the formation of the hydroxyl radical during the photolysis of Fe^{3+}_{aq} at pH 3.0 exists. This reaction pathway, which shows a quantum yield of 0.21, is suppressed in the presence of most organic compounds dissolved in water, because the quantum yields for the photooxidation of iron(III)-coordinated organic ligands are usually significantly higher. In this work, quantum yields for the oxidation of 2,4-xylidine ($\Phi = 0.92$) and H_2O_2 ($\Phi = 1.33$) by electronically excited iron(III) have been measured for the first time. The observed reaction behavior is summarized in Table 5.

Acknowledgment. Financial support from Hewlett-Packard is gratefully acknowledged. L.P. Jr. thanks the United Nations for a grant supporting his Ph.D. thesis. A part of this research has also been funded by BMBF.

References and Notes

(1) (a) Legrini, O.; Oliveros, E.; Braun, A. M. *Chem. Rev.* **1993**, *93*, 671−698 and references therein. (b) Ollis, D. F.; Al-Ekabi, H., Eds. *Photocatalytic Purification and Treatment of Water and Air*; Elsevier: Amsterdam, 1993.

(2) Buxton, G. V.; Greenstock, C. L.; Helman, W. P.; Ross, A. B. *J. Phys. Chem. Ref. Data* **1988**, *17*, 513−886.

(3) (a) Fenton, H. J. H. *J. Chem. Soc.* **1894**, *65*, 899−901. (b) Fenton, H. J. H. *J. Chem. Soc., Trans.* **1899**, *75*, 1−11. (c) Walling, C. *Acc. Chem. Res.* **1975**, *8*, 125−131.

(4) (a) Cahill, A. E.; Taube, H. *J. Am. Chem. Soc.* **1952**, *74*, 2312−2316. (b) Eisenhauer, H. R. *J. WPCF* **1964**, *36*, 1116−1128. (c) Bishop, D. F.; Stern, G.; Fleischman, M.; Marshall, L. S. *Ind. Eng. Chem. Proc. Design Dev.* **1968**, *7*, 110−117. (d) Pasek, E. A.; Straub, D. K. *Inorg. Chem.* **1972**, *11*, 259−266. (e) Feuerstein, W.; Gilbert, E.; Eberle, S. H. *Vom Wasser* **1981**, *56*, 35−54. (f) Barbeni, M.; Minero, C.; Pelizzetti, E.; Bogarello, E.; Serpone, N. *Chemosphere* **1987**, *6*, 2225−2237. (g) Sedlak, D. L.; Andren, A. W. *Environ. Sci. Technol.* **1991**, *25*, 777−782. (h) Lipczynska-Kochany, E. *Chemosphere* **1991**, *22*, 529−536.

(5) (a) Goldstein, S.; Czapski, G.; Meyerstein, D. *Free Radicals Biol. Med.* **1993**, *15*, 435−445. (b) Ruppert, G.; Bauer, R.; Heisler, G. *J. Photochem. Photobiol. A: Chem.* **1993**, *73*, 75−78. (c) Andrianirinaharivelo, S.; Mailhot, G.; Bolte, M. *Solar Energy Mater. Solar Cells* **1995**, *38*, 459−474. (d) Safarzadeh-Amiri, A.; Bolton, J. R.; Cater, S. R. *Solar Energy* **1996**, *56*, 439−444. (e) Bandara, J.; Morrison, C.; Kiwi, J.; Pulgarin, C.; Peringer, P. *J. Photochem. Photobiol. A: Chem.* **1996**, *99*, 57−66. (f) Pignatello, J. J.; Chapa, G. *Environ. Toxicol. Chem.* **1994**, *13*, 423−427. (g) Pignatello, J. J. *Environ. Sci. Technol.* **1992**, *26*, 944−951. (h) Sun, Y.; Pignatello, J. *J. Agric. Food Chem.* **1993**, *41*, 1139−1142. (i) Safarzadeh-Amiri, A.; Bolton, J. R.; Cater, S. R. *J. Adv. Oxid. Technol.* **1996**, *1*, 18−26.

(6) (a) Oliveros, E.; Legrini, O.; Braun, A. M.; Hohl, M.; Müller, T. *Water Sci. Technol.* **1997**, *35*, 223−230. (b) Oliveros, E.; Legrini, O.; Hohl, M.; Müller, T.; Braun, A. M. *Chem. Eng. Proc.* **1997**, *36*, 397−405.

(7) (a) Haber, F.; Weiss, J. J. *Proc. R. Soc. London, Ser. A* **1934**, *147*, 332−345. (b) Merz, J. H.; Waters, W. A. *Discuss. Faraday Soc.* **1949**, *2*, 179−182.

(8) (a) Barb, W. G.; Baxendale, J. H.; George, P.; Hargrave, K. R. *Trans Faraday Soc.* **1951**, *47*, 462−500. (b) Barb, W. G.; Baxendale, J. H.; George, P.; Hargrave, K. R. *Trans. Faraday Soc.* **1951**, *47*, 591−616.

(9) (a) Goldstein, S.; Czapski, G.; Meyerstein, D. *Free Radicals Biol. Med.* **1993**, *15*, 435−445. (b) Marsarwa, M.; Cohen, H.; Meyerstein, D.; Hickman, D. L.; Bakac, A.; Espensen, J. H. *J. Am. Chem. Soc.* **1988**, *110*, 4293−4297.

(10) Cotton, F. A.; Wilkinson, G. *Advanced Inorganic Chemistry;* Verlag Chemie: Weinheim, Germany, 1980; pp 461−488.

(11) Wink, D. A.; Nims, R. W.; Saavedra, J. E.; Utermahlen, W. E.; Ford, P. C. *Proc. Natl. Acad. Sci. U.S.A.* **1994**, *91*, 6604−6608.

(12) Rush, J. D.; Bielski, H. J. *J. Am. Chem. Soc.* **1986**, *108*, 523−525.

(13) Kremer, M. L.; Stein, G. *Trans. Faraday Soc.* **1959**, *55*, 595−560.

(14) Luzzatto, E.; Cohen, H.; Stockheim, C.; Wieghardt, K.; Meyerstein, D. *Free Radical Res.* **1995**, *23*, 453−463.

(15) Sychev, A. Y.; Isaak, V. G. *Russ. Chem. Rev.* **1995**, *64*, 1105−1129.

(16) Sun, Y.; Pignatello, J. J. *Environ. Sci. Technol.* **1993**, *27*, 304−310.

(17) Wiberg, N.; Wiberg, E.; Hollemann, A. F. *Lehrbuch der Anorganischen Chemie*; Walter de Gruyter: Berlin, New York, 1985; pp 1136−1139.

(18) Koppenol, W. H.; Liebman, J. F. *J. Phys. Chem.* **1984**, *88*, 99−101.

(19) (a) Sonntag, C. v.; Schuchmann, H.-P. *Angew. Chem.* **1991**, *103*, 1255−79. (b) Turro, N. J. *Modern Molecular Photochemistry*; University Science Books: Mill Valley, CA, 1991.

(20) (a) Sawyer, D. T.; Kang, C.; Llobet, A.; Redman, C. *J. Am. Chem. Soc.* **1993**, *115*, 5, 5817−5818. (b) Hage, J. P.; Llobet, A.; Sawyer, D. T. *Bioorg. Med. Chem.* **1995**, *3*, 1383−1388.

(21) (a) Balzani, V. C.; Carassiti, V. *Photochemistry of Coordination Compounds*; Academic Press: New York, 1970. (b) Hennig, H.; Rehorek, D. *Photochemische und Photokatalytische Reaktionen von Koordinationsverbindungen*; Akademie Verlag: Berlin, 1987.

(22) Walling, C.; Goosen, A. *J. Am. Chem. Soc.* **1973**, *95*, 2987−2991.

(23) (a) Langford, C. H.; Carey, J. H. *Can. J. Chem.* **1975**, *53*, 2430−2435. (b) Faust, B. C.; Hoigne, J. *J. Atm. Environ.* **1990**, *24*, 79−89. (c) Zuo, Y.; Hoigné, J. *Environ. Sci. Technol.* **1992**, *26*, 1014−1022.

(24) Dobereiner, J. *Schw. J.* **1833**, *62*, 90−92.

(25) Jander, G.; Blasius, E. *Einführung in das anorganisch-chemische Praktikum*; Hirzel: Stuttgart, Germany, 1984.

(26) Braun, A. M.; Maurette, M.-T.; Oliveros, E. *Photochemical Technology*; Wiley & Sons: New York, Chichester, U.K., 1991; pp 76−80 and references therein.

(27) (a) Christen, H. R. *Grundlagen der Organischen Chemie*; Otto Salle Verlag: Frankfurt/Main, Germany, 1982. (b) Gontier, S.; Tuel, A. *J. Catal.* **1995**, *157*, 124−132. (c) Tonti, S.; Roffia, P.; Cesana, A.; Mantegazza, M.; Padovan, M. *Eur. Pat.* **1988**, *314*, 147−155. (d) Sakaue, S.; Tsubakino, T.; Nishiyama, Y.; Ishii, Y. *J. Org. Chem.* **1993**, *58*, 3633−3642. (e) Werkert, E.; Angeli, E. *Synth. Commun.* **1988**, *18*, 1331−1339. (f) Tollari, S.; Vergani, D.; Banfi, S.; Porta, F. *J. Chem. Soc., Chem. Commun.* **1993**, 442−451. (g) Donten, M.; Hyk, W.; Ciszkowska, M.; Stojek, Z. *Electroanalysis (Weinheim)* **1997**, *9*, 751−754. (h) Hoon, M.; Fawcett, R. W. *J. Phys. Chem. A* **1997**, *101*, 3726−3730. (i) Spitsyn, M. A.; Andreev, V. N.; Kazarinov, V. E. *Russ. J. Electrochem.* **1995**, *31*, 1092−1097. (k) Wang, L.; Goodloe, G. W.; Stallman, B. J.; Cammarata, V. *Chem. Mater.* **1996**, *8*, 1175−1181.

(28) The value of $E \approx 2.43$ V was estimated using Fe^{3+}_{aq} ($E \approx 0.66$ V at pH 3.0) and $E_{0-0} = 1.77$ V, corresponding to λ_{0-0} (Fe^{3+*}_{aq}) = 700 nm at pH 3.0.

(29) Maillard, C.; Guillard, C.; Pichat, P. *Chemosphere* **1992**, *24*, 1085−1094 and references therein.

(30) Cotton, F. A. *Coord. Chem. Rev.* **1972**, *8*, 185−227.